Applied Catalysis B: Environmental 101 (2011) 495–503

Contents lists available at ScienceDirect

Applied Catalysis B: Environmental

journal homepage: www.elsevier.com/locate/apcatb

Esterification of oleic acid over solid acid catalysts prepared from Amazon *flint* kaolin

Luís Adriano S. do Nascimento[a], Laura M.Z. Tito[a], Rômulo S. Angélica[b], Carlos E.F. da Costa[a], José R. Zamian[a], Geraldo N. da Rocha Filho[a,*]

[a] Laboratório de Catálise e Oleoquímica, Universidade Federal do Pará, Rua Augusto Corrêa, Guamá, CEP 66075-11, Belém, Pará, Brazil
[b] Laboratório de Difração de Raios-X, Universidade Federal do Pará, Rua Augusto Corrêa, Guamá, CEP 66075-11, Belém, Pará, Brazil

ARTICLE INFO

Article history:
Received 24 June 2010
Received in revised form
25 September 2010
Accepted 19 October 2010
Available online 26 October 2010

Keywords:
Acid activation
Metakaolin
Microporous
Esterification
Oleic acid

ABSTRACT

The esterification of free fatty acids (FFA) can be used to produce biodiesel from high FFA oils. In this work, a new eco-friendly catalyst for the esterification of oleic acid with methanol has been prepared from a waste material, Amazon *flint* kaolin, that was thermally treated (at 850 and 950 °C) and activated with sulfuric acid solutions (1 M and 4 M). The activated metakaolin samples were characterized by X-ray diffraction, scanning electron microscopy, N_2 adsorption–desorption and adsorption studies of pyridine using TG/DTG and FTIR analysis. The leached metakaolin treated at 950 °C and activated with 4 M sulfuric acid solution showed the highest surface area (406 m^2/g), the highest number of acid sites (237.7 μmol/g) and offered the maximum esterification activity (98.9%) at 160 °C, an acid:methanol molar ratio of 1:60 and 4 h reaction time. The influences of reaction parameters such as the molar ratio of the reactants, alcohol chain length, temperature and time have also been investigated. Based on the catalytic results, Amazon *flint* kaolin is found to be a promising raw material for the production of new solid acid catalysts for the esterification of FFAs.

1. Introduction

Clays are very versatile materials that can be used as adsorbents, ion exchangers, decolorizing agents, catalyst supports and catalysts [1]. Clay-catalysts are interesting materials, not only for the low cost of the raw material [2], but also for their lack of harmful effects on the environment [3].

The study of modified clays has attracted interest due to the structure and dimension of their pores, which appear to be suitable for the conversion of large molecules [4]. Acid-activation is one of the modifications that can be made to clays [5–7]. It causes the disaggregation of clay particles, elimination of impurities and dissolution of external layers, altering the chemical composition and structure of clays [8]. The main consequences of acid activation are an increase of surface area, porosity and number of acid sites compared to the parent clays [4].

Acid-activated clays are considered as efficient solid catalysts, not only due to their strong acid sites, but also due to their part-amorphous nature that provides a wide range of pore sizes [9]. For these reasons, microporous or mesoporous acid-activated metakaolins have been reported as efficient catalysts for isomerization, Friedel–Crafts alkylation and dehydration reactions [4,10,11]. It is also important to note that acid-treated clays remain one of the most important classes of acid solid catalysts available in the industry [1]. For example, acid-treated montmorillonites are offered by various companies as catalysts for hydrocarbon cracking, as is the well-known commercial montmorillonite clay K-10, the surface acidity and catalytic activity of which can be enhanced considerably by exchanging with transition metal ions [12]. However, the catalytic activity of another major group of clay minerals, kaolinite, has not been studied as thoroughly.

The Amazon region, specifically the Northeast of Pará state, possesses the largest Brazilian reserves of high-whiteness kaolin [13]. The kaolin is inserted in the context of the Ipixuna Formation, where is possible to distinguish two main units (Inferior and Superior Units) [14]. The Inferior Unit is formed mainly of kaolin and in whose base is found the *soft* kaolin that is used in paper coating and on top of which there is the *flint* or *semi-flint* kaolin (Fig. 1) [15]. *Flint* kaolin is not used by the kaolin industry, as it is iron-rich, increasing the cost of extraction and separation from the *soft* kaolin [13]. Regarded as a waste byproduct, *flint* kaolin also represents an environmental cost resulting from the production of kaolin, making it necessary to find ways to use this material to minimize the impacts caused by this process on the environment.Considering these facts, Amazon *flint* kaolin can be considered an interesting, low-cost material that can be tested as the raw mate-

* Corresponding author. Tel.: +55 91 32018032; fax: +55 9132018032.
E-mail address: narciso@ufpa.br (G.N. da Rocha Filho).

0926-3373
doi:10.1016/j.apcatb.2010.10.021

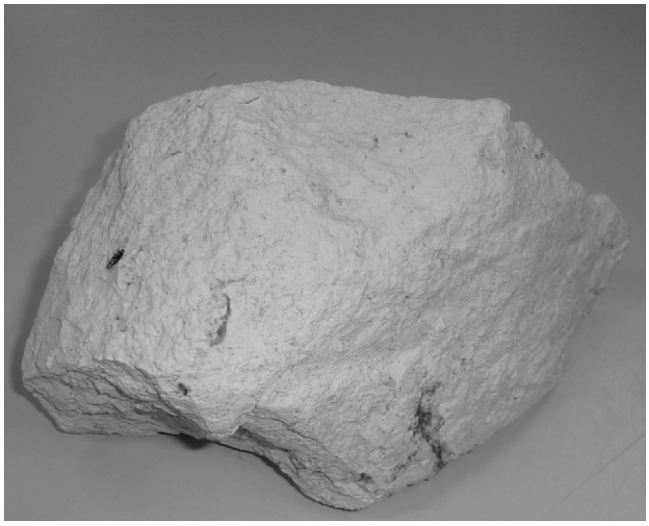

Fig. 1. A photograph of a representative sample of Amazon *flint* kaolin used in this work.

rial for a new solid acid catalyst.Among the branches of chemistry that require the use of acid catalysts is the production of sustainable alternative fuels, which has attracted both academic and industrial interest. Biodiesel is one of these sustainable fuels and is a non-petroleum-based fuel with many advantages, including low emissions, biodegradability and increased lubricity [16]. Biodiesel consists of alkyl esters derived from either the transesterification of triglycerides (TGs) in oils and fats or the esterification of free fatty acids (FFAs) with short-chain alcohols [16,17].One drawback of the production of biodiesel by transesterification is that the utilization of high FFA acid feeds in traditional biodiesel production leads to depletion of the catalysts and increased purification costs because the free fatty acid is saponified by the homogeneous alkaline catalyst, producing excess soap [18]. Esterification of FFA to alkyl esters in the presence of an acidic catalyst can improve the use of high FFA oils in biodiesel production [19]. Esterification is normally carried out in the homogeneous phase in the presence of acid catalysts such as H_2SO_4, HF, H_3PO_4, HCl and *p*-toluene sulfonic acid [19,20]. This pretreatment step has been successfully demonstrated using sulfuric acid [21]. Unfortunately, use of the homogeneous sulfuric acid catalyst adds neutralization and separation steps to the process in addition to the esterification reaction [22]. Moreover, these catalysts have problems when used because they are hazardous and generate polluting, corrosive liquid acids [20]. Therefore, the use of heterogeneous catalysts can be considered an alternative that can minimize environmental damage and reduce the cost of biodiesel. Several studies relate to the production of catalysts as sulfonated carbons [23,24], modified zirconias [25,26], mesoporous sulfonic acid [27], heteropolyacid-based catalysts [28] and MCMs [19]. However, no articles have been published regarding the use of catalysts for the esterification reaction prepared using Amazon *flint* kaolin, a raw material considered waste.

This study reports the preparation and characterization of acid-leached metakaolins from Amazon *flint* kaolin and their utilization as catalysts for the esterification reaction of oleic acid with short-chained alcohols.

2. Experimental

2.1. Materials

Oleic acid (synthetic grade) was purchased from Aldrich, methanol and ethanol were purchased from Synth and 1-propanol was purchased from Vetec. All alcohols were of AR grade. The *flint* kaolin used was collected in a mine located in the area around Rio Capim (Pará-Brazil). The *flint* kaolin was triturated, and the sandy fraction was separated for retention in a sieve. The fraction below 62-μm particle size was then collected, diluted in distilled water and centrifuged for separation of the silt fraction, thereby obtaining the clay fraction.

2.2. Methods

2.2.1. Thermal treatment and acid activation of Amazon flint kaolin

The amounts of SiO_2, Al_2O_3 and H_2O present in *flint* kaolin are almost the same as the theoretical values obtained for kaolinite. *Flint* kaolin is therefore constituted mainly by kaolinite. We also observed a high Fe_2O_3 and TiO_2 content, which could be related to the presence of accessory minerals (such as hematite and anatase) and/or the presence of Al isomorphically substituted in both cases [13].

Kaolin is resistant to acid leaching due to its high octahedral aluminum content, and the transformation of kaolin into metakaolin would increase the susceptibility of the former to the aluminum and iron cations leaching from the octahedral layer [4]. The phase transformations that occur when *flint* kaolin is calcined at high temperatures are demonstrated by the chemical reactions illustrated below [13].

$$\underset{\text{Kaolinite}}{2SiO_2 \cdot Al_2O_3 \cdot 2H_2O} \xrightarrow[\sim 537\ ^\circ C]{} \underset{\text{Metakaolinite}}{2SiO_2 \cdot Al_2O_3} + 2H_2O(g)$$

$$\underset{\text{Metakaolinite}}{2SiO_2 \cdot Al_2O_3} \xrightarrow[\sim 983\ ^\circ C]{} \underset{\text{Primary 1 : 1 mullite (Al–Si spinel)}}{Al_2O_3 \cdot SiO_2} + \underset{\text{(amorphous)}}{SiO_2}$$

Samples of the clay fraction of *flint* kaolin were calcined at 850 and 950 °C, providing metakaolin samples that were labeled as MF8 and MF9, respectively. Both the MF8 and the MF9 samples were activated at 90 °C for 1 h with 1 M and 4 M sulfuric acid solutions, and then washed with distilled water, dried at 120 °C for 12 h and calcined at 400 °C for 2 h. The four obtained metakaolin samples were designated as MF8S1, MF8S4, MF9S1 and MF9S4.

2.2.2. Characterization

The chemical composition analysis was performed using a Shimadzu Ray ny EDX-700 energy dispersive X-ray (EDX) spectrometer.

X-ray diffractions were obtained using a PANalytical X′PERT PRO MPD (PW 3040/60) diffractometer, using the powder method, at $5^\circ\langle 2\theta\rangle 70^\circ$ intervals. CuKα (40 kV and 40 mA) radiation was used. The 2θ scanning speed was 0.02°/s.

N_2 adsorption–desorption isotherms were obtained at liquid nitrogen temperature using a Quantachrome Nova 1200 apparatus. Before each measurement, the samples were outgassed at 130 °C for 2 h. The specific surface area, the microporous area, the microporous volume and the pore-size distribution were obtained, respectively, using Brunauer-Emmett–Teller (BET), *t*-plot and Barrett–Joyner–Halenda (BJH) methods.

The powder mesh size of the prepared catalysts was determined on FRITSCH equipment, model ANALYSETTE 22 MICROTEC PLUS. The data were treated using Milling and Sizing Control Software.

The morphology of the samples was inspected using a ZEISS microscope, model LEO 1430, operating at 10 kV and 90 mA. The samples were supported on carbon tapes and metalized with gold under vacuum conditions.

Thermogravimetry (TG) and derivative thermogravimetry (DTG) have been extensively used in catalyst characterization, because they allow for quick evaluation of material changes in

Table 1
Chemical compositions of the major components of kaolinite, *flint* kaolin and the leached metakaolins.

	Theoretical kaolinite	*Flint*	MF8S1	MF8S4	MF9S1	MF9S4
SiO_2	46.54	43.24	54.32	63.65	53.51	61.84
Al_2O_3	39.50	37.98	34.20	23.63	32.20	16.90
TiO_2	–	2.34	3.88	2.84	3.72	4.43
Fe_2O_3	–	0.51	0.60	1.53	0.57	0.45
Loss on ignition at 1000 ± 25 °C (wt.%)	13.96	15.40	6.70	8.07	9.46	16.25

response to temperature variations [29,30]. The literature shows that pyridine is a suitable probe to measure the surface acidity of porous materials and is able to provide quantitative analysis of the acid sites by Temperature-Programmed Desorption (TPD) [29,31–33]. Furthermore, FTIR of adsorbed pyridine has become routine in catalysis laboratories and can differentiate Brønsted, Lewis and hydrogen-bonded sites [29,34].

Based on this, the acidity studies at this work were performed using the methodology described by Ghesti et al. [29] using TG/DTG and FTIR after pyridine adsorption, and proved to be a good tool for characterization of the TPD profiles of heterogeneous catalysts [29].

Approximately 100 mg of each sample was dehydrated at 400 °C in an N_2 flow (40 cm^3/min) for 90 min, cooled to 120 °C, and gaseous pyridine (diluted in N_2) was then passed through the samples for 30 min. The temperature was kept at 120 °C under N_2 flow for 60 min to remove the physically adsorbed pyridine. Subsequently, the samples were analyzed by TG/DTG and FTIR.

Thermogravimetric analyses were performed in a N_2 flow (40 cm^3/min) over the temperature range of 25–900 °C, at a heating rate of 10 °C/min, using a SHIMADZU thermobalance (TG/DTA), model DTG-60H.

The number of acid sites was calculated as follows: (i) From the total weight (w_{total}) of a sample with adsorbed pyridine (sample Py) analyzed by TG/DTG, we subtracted the weight lost between 25 and 250 °C (w_{250}, usually water and/or physically adsorbed pyridine), thereby obtaining the anhydrous weight of the sample; (ii) the amount of weight lost between 250 and 900 °C (w_{Py}, chemically adsorbed pyridine) was normalized for 1 g, dividing the value obtained by the anhydrous weight; (iii) the same calculation was accomplished using the curve of TG/DTG for the sample without adsorbed pyridine; (iv) the weight of adsorbed pyridine is equal to the difference between the normalized values for the sample with and without adsorbed pyridine; (v) using the pyridine molar weight (MWPy), we determined the number of moles of adsorbed pyridine. These procedures are mathematically represented using the equation adapted from Macedo [31] below:

$$n_{Py} = \frac{\{[w_{Py}/(w_{total} - w_{250})]_{\text{Sample with Py}} - [w_{900}/(w_{total} - w_{250})]_{\text{Sample without Py}}\}}{MW_{Py}}$$

where w_{900} = weight lost between 250 and 900 °C.

Infrared spectra were recorded in the 4000–500 cm^{-1} spectral region using a Thermo IR100 spectrometer.

2.2.3. Catalytic tests

Before the experiments, the catalysts were activated at 200 °C in an oven for 2 h. The catalytic tests were performed using a PARR 4843 reactor. In a typical experiment, oleic acid was mixed with methanol and 5% of the solid acid catalyst (related to acid weight). The reaction mixture was kept under constant stirring (500 rpm) at 130 °C for 2 h. After the reaction was complete, the solid catalyst was separated by filtration. The percent of conversion of oleic acid into its ester was estimated by measuring the acid value of the product by titration with sodium hydroxide. The conversion of FFA was calculated by the formula:

$$x_{ffa}(\%) = \left[\frac{(a_i - a_t)}{a_i}\right] \times 100$$

where a_i is the initial acidity of the mixture and a_t is the acidity at a "t" time.

The effects of alcohol chain length, the molar ratio of the reactants, temperature and time on the esterification of oleic acid were investigated using the most active catalyst.

3. Results and discussion

3.1. Characterization

3.1.1. Chemical compositions and XRD

The chemical compositions of the *flint* kaolin and leached metakaolins were determined using EDX, and the values are compared with those of theoretical kaolinite [13] in Table 1.

The XRD of *flint* kaolin (Fig. 2A) showed the characteristic signals of kaolinite at 2θ values of 12° and 24° [13]. The absence of the three well-resolved signals in the range of 20°⟨2θ⟩24° revealed the low order degree of the *flint* kaolin. All the leached metakaolins exhibited similar X-ray diffractograms (Fig. 2B). When the samples were calcined at 850 °C and 950 °C for 2 h, water was lost and the kaolinite peaks disappeared. The signals were replaced by a broad band between 15°⟨2θ⟩25°, which can be attributed to an amorphous phase of SiO_2 [4]. We also observed the presence of three intense peaks at 2θ values of 25°, 37.8° and 48° that were related to anatase (TiO_2), frequently found as an accessory mineral in the kaolin of the Capim region and in other kaolins [13]. We also observed the presence of components of the parent clay such as cristobalite (SiO_2) and other minerals, including quartz and hematite (Fe_2O_3). The XRD analysis also revealed a complete breakdown of the crystalline structure of the leached metakaolins compared to the parent kaolin and a structural water loss that facilitated the transformation of octahedral AlO_6 into tetra- and penta-coordinated Al units. The literature reports that these Al units are more reactive and more susceptible than hexa-coordinated Al units to the acid leaching that is responsible for the partial dissolution of Al^{3+} and, consequently, for the observed increase of the amorphous phase [4,10,11].

3.1.2. Scanning electron microscopy (SEM)

SEM micrographs of *flint* kaolin and one of the leached metakaolins (Fig. 3) showed that both *flint* kaolin and the leached metakaolin had particles with sizes below 1 μm. *Flint* kaolin is formed mainly by the stacking of flaky particles with a pseudo-hexagonal morphology. The SEM study also showed that the leached metakaolin is formed by agglomerates of particles with rough surfaces and porosity related to the spaces between these agglomerates.

3.1.3. N_2 adsorption–desorption and powder mesh size

The type II (IUPAC classification) N_2 adsorption–desorption isotherms (Fig. 4A) and the pore size distribution curves (Fig. 4B) of the acid-activated metakaolins show that these materials have microporous structures and surface area values that are higher than

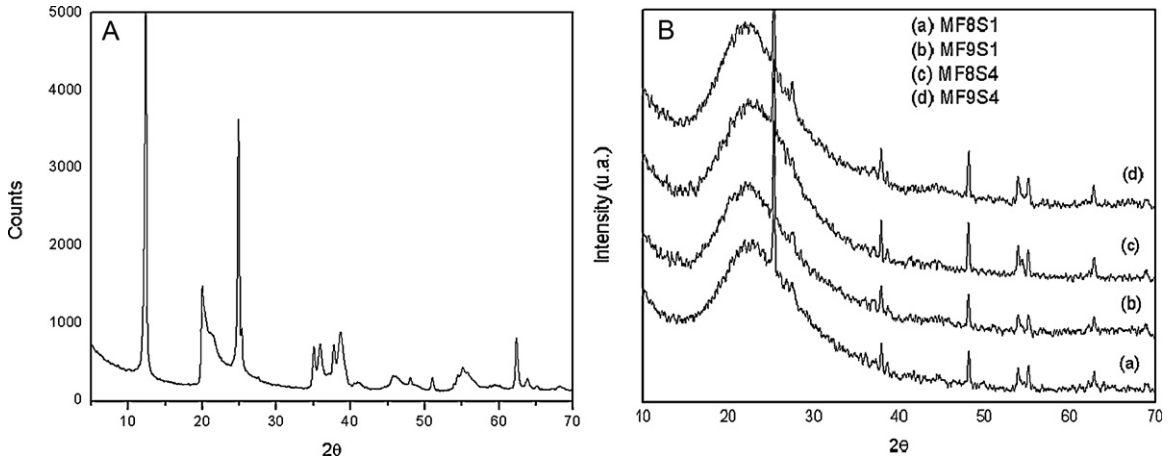

Fig. 2. X-ray diffractograms of: (A) *flint* kaolin; (B) the leached metakaolins.

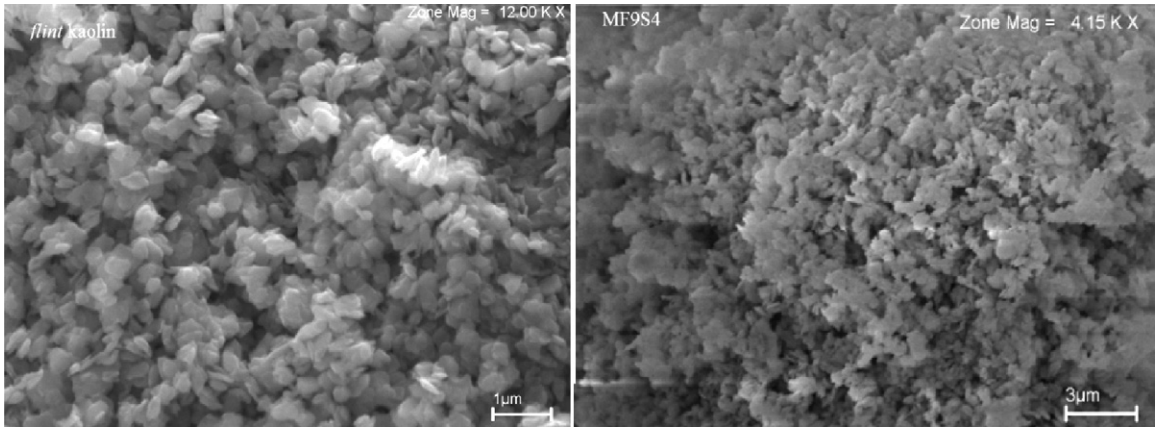

Fig. 3. SEM micrographs for *flint* kaolin (left) and MF9S4 (right).

those of *flint* kaolin (Table 2). This results from acid leaching and, consequently, the presence of amorphous silica in the sample, with MF9S4 presenting the largest surface area (406 m^2/g).

Considering that the microporous area and the microporous volume of the leached metakaolins also increased (this was influenced directly by the preparation conditions), some of the acid-treated metakaolins could be considered interesting from a catalytic point of view, because in previous studies using other kaolins, materials that were produced with similar behavior presented catalytic activity [10,11].

The measured values of powder mesh size shown that the samples MF9S4 and MF8S4 present particles smaller than MF9S1 and MF8S1. These results are coherent with surface area values of each sample.

The specific surface areas, microporous areas, microporous volumes and powder mesh sizes are presented in Table 2.

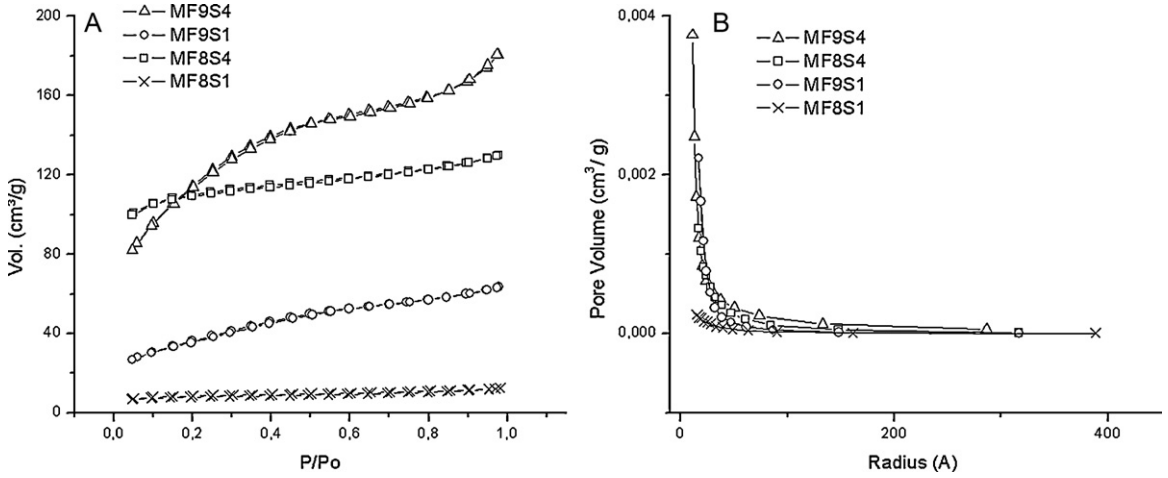

Fig. 4. N_2 adsorption–desorption isotherms (A) and pore distribution (B) of the acid-activated metakaolins.

Table 2
The specific surface areas, microporous areas, microporous volumes and powder mesh size of *flint* kaolin and the leached metakaolins.

Sample	S.A.[a] (m^2/g)	$A\mu$[b] (m^2/g)	$V\mu$[c] (cm^3/g)	P.M.S.[d] (particles up to 6.4 μm)
Flint kaolin	24	11.5	0.006	–
MF9S4	406	319	0.15	84.7%
MF9S1	76	54	0.046	58.7%
MF8S4	341	313	0.16	84.1%
MF8S1	27	22	0.011	58.6%

[a] Specific surface area calculated by BET.
[b] $S\mu$ = Microporous area calculated based on the *t*-plot.
[c] $V\mu$ = Microporous volume calculated based on the *t*-plot.
[d] Powder mesh size.

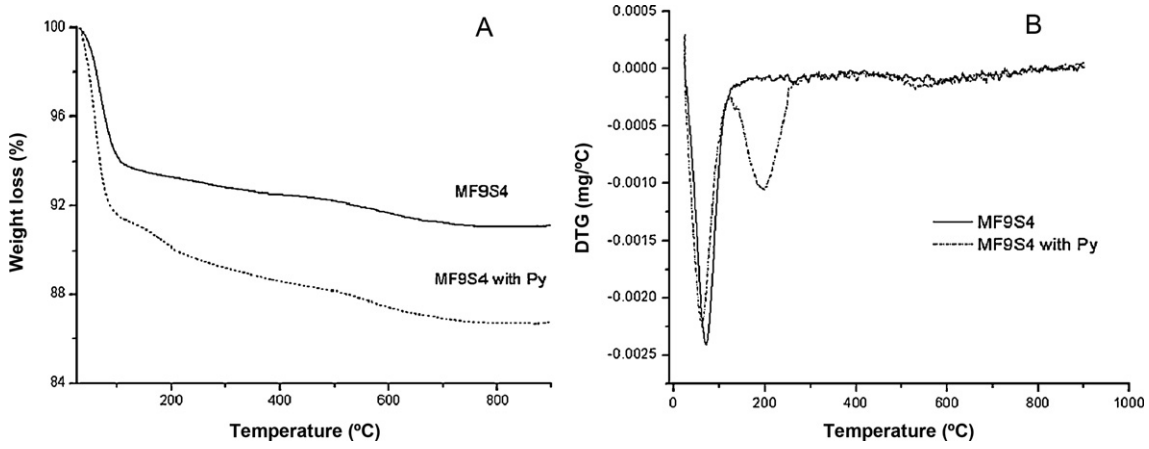

Fig. 5. Curves of MF9S4 with and without adsorbed pyridine: (A) TG and (B) DTG.

3.1.4. The acidity of activated metakaolins

The TG curves for all the leached metakaolins showed a behavior similar to that described by Belver et al. [8], presenting two different processes: a fast loss at temperature between 25 and 100 °C, associated with adsorbed water, and a second, continuous loss between 250 and 900 °C attributed to dehydroxylation from the $Si(OSi)_3OH$ groups formed during the treatment or to water molecules fixed on specific sites of the solids, probably coordinated to the remaining Al cations.

The largest weight loss was observed for MF9S4, as it had the largest amount of amorphous silica in its composition, increasing the number of adsorbed water molecules on the surface. The TG curves indicated that the samples with adsorbed pyridine lost more weight than the samples without adsorbed pyridine; this is exemplified using the curves for MF9S4 in Fig. 5. The TG/DTG curves of sample with adsorbed pyridine present a loss between 150 and 250 °C which can be assigned to physically adsorbed water and pyridine, and a continuous loss above 250 °C attributed to loss of chemically adsorbed pyridine.

From Table 3, we observe that the acidity of each material resulted directly from the preparation conditions, as the samples prepared with sulfuric acid 4 M had a higher density of acidic sites. These results are in agreement with those obtained by Sabu et al. [11], who reported that treating metakaolin with acid results in the relocation of Al cations from the structure to the newly created pores. The cations act as Brönsted acid centers in the presence of water and as Lewis acid centers under anhydrous conditions.

Fig. 6 shows the relation between the density of acidic sites and the surface area of the activated metakaolins, confirming that the concentration of acid contributes greatly to the final properties of the leached metakaolins.

The infrared spectra in the region from 1700 to 1400 cm^{-1} of the samples with adsorbed pyridine (Fig. 7) show typical bands that can be assigned to Lewis site-bonded pyridine (at approximately 1446 and 1629 cm^{-1}), and Brönsted site-bonded pyridine at 1535 and 1635 cm^{-1}. There is also a band at approximately 1492 cm^{-1} that can be attributed to the pyridine molecules associated with both Brönsted and Lewis acidic sites, and this profile agrees with that presented by other leached metakaolins [10], confirming the nature of the acidic sites of the acid-activated metakaolins.

Table 3
Evaluation of the number of acid sites in the leached metakaolins.

Sample	Number of acid sites (μmol Py/g)
MF9S4	237.7
MF9S1	72
MF8S4	147.4
MF8S1	35.5

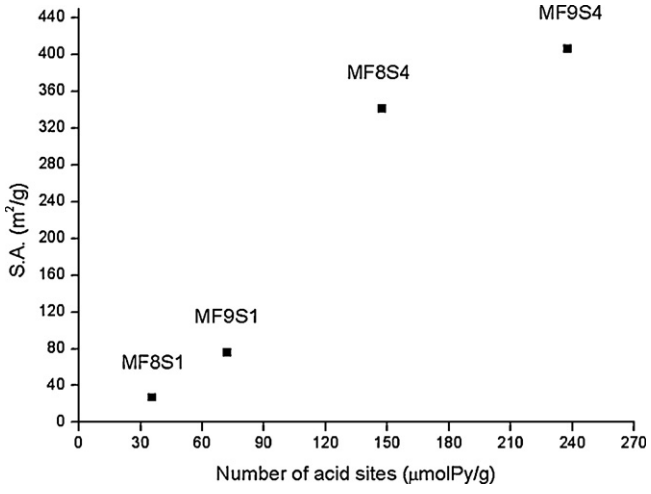

Fig. 6. The number of acid sites versus the surface area of the leached metakaolins.

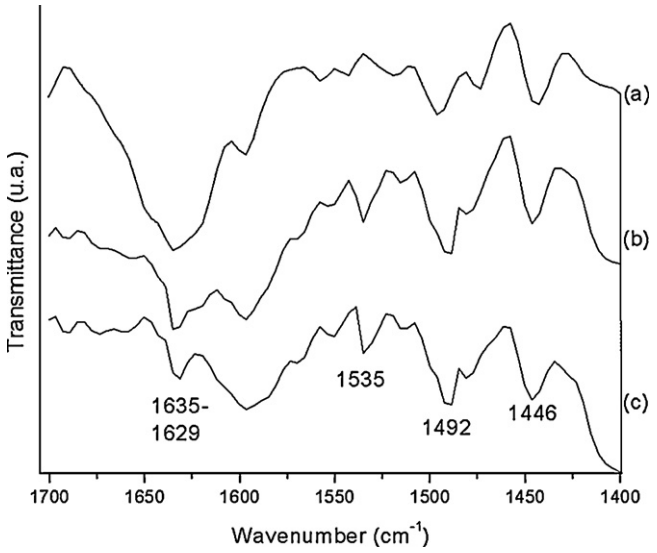

Fig. 7. IR spectra in the region 1700–1400 cm^{-1} of MF9S4 (a) without adsorbed pyridine and (b) with adsorbed.

3.2. Catalytic tests

The catalytic activity of the acid-activated metakaolins for the esterification of oleic acid was determined from the acidity index of the final product. Fig. 8 shows the effect of each catalyst on the esterification reaction with methanol.

The analysis of the results obtained shows that the final conversion rate is related directly to the increase in surface area and to the decrease in the concentration of Al in the sample. This supplies a wider distribution of Al across the surface of the leached metakaolin and facilitates access of the reactants to the catalytic sites, resulting in a larger conversion value. This explains the significantly greater performance of MF9S4 as a catalyst, which also can be attributed to its greater number of acidic sites.

In fact, MF8S4 presented the best catalytic activity after MF9S4, revealing that their different performance is probably should be related to the fact that *flint* kaolin calcined at 950 °C is more susceptible to acid leaching than that calcined at 850 °C, i.e., the highest temperature produced more tetra- and penta-coordinated Al units and a greater amount of amorphous silica [8,35]. This also can explain the similar activity of MF9S1 and MF8S1.

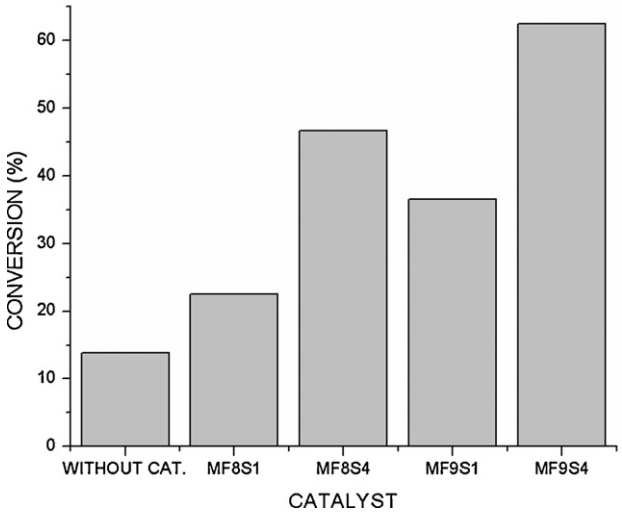

Fig. 8. Conversion at 130 °C, oleic acid: methanol (1:60), time: 120 min.

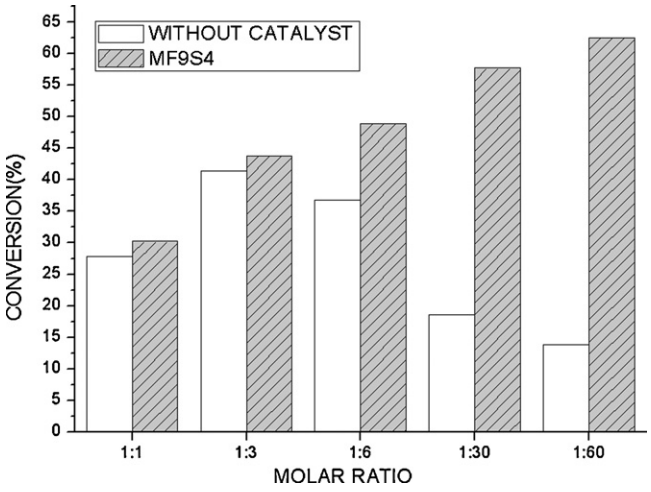

Fig. 9. The effect of the molar ratio of the reactants on the conversion. Temperature: 130 °C, time: 120 min.

3.2.1. The effect of the molar ratio of the reactants on the conversion

Because of the result of the first catalytic tests, we chose to test MF9S4 as a catalyst in the esterification of oleic acid with methanol, using other reactant molar ratios. The reactions used acid:alcohol molar ratios of 1:1, 1:3, 1:6, 1:30 and 1:60, and the results are shown in Fig. 9.

We increased the amount of alcohol, as we observed that the conversion rate increased at an acid:alcohol ratio of 1:3. In reactions without catalyst at acid:alcohol molar ratios greater than 1:6, we observed a decrease in the conversion rate that can be attributed to the formation of a greater amount of water, moving the equilibrium in the direction of the inverse reaction. In reactions with MF9S4, we observed different behaviors: additional alcohol in the reactants greatly improved the conversion rate. This can be explained by considering that the increasing number of alcohol molecules around the catalyst could facilitate the removal of water molecules from the surface of the catalyst, increasing their catalytic activity, because the use of acid-treated clays is restricted to nonaqueous systems [36].

3.2.2. The effect of alcohol chain length

The effect of alcohol chain length on the esterification process was studied, and the result is shown in Fig. 10. The effectiveness

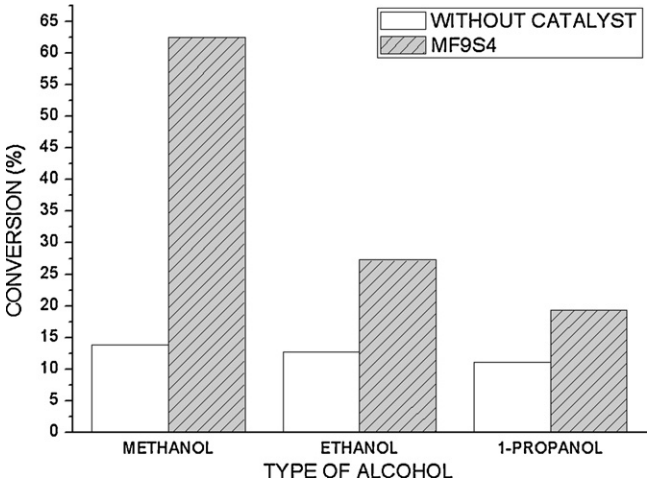

Fig. 10. The effect of alcohol chain length on the conversion. Temperature: 130 °C, time: 120 min, oleic acid:alcohol (1:60).

of the esterification of oleic acid was: methanol (62.5%) > ethanol (27.3%) > 1-propanol (19.4%). Carmo et al. [19] described similar results for the esterification of palmitic acid using Al-MCM-41 as a catalyst. The effect of the size and type of the alcohol chain on esterification was reported by Kirumakki et al. [37] for the zeolites: H-beta, HY, and HZSM-5. Although each alcohol has a different reactivity, it is important to note that the microporous nature of MF9S4 may be important, because the efficiency using methanol was much higher than those obtained with ethanol or 1-propanol. Zaidi et al. [38] presented two explanations for such behavior. The first one is related to alcohol nucleophilicity, suggesting that the greater the number of carbon atoms, the lowest the alcohol nucleophilicity. As a result, the reaction rate decreases. According to the authors, the steric effect may also explain this behavior, because as the alcohol length chain becomes larger, the approaching to the catalyst becomes more difficult.

3.2.3. The effect of temperature

The normal behavior for the catalyzed reactions is that the conversion rate increases with temperature [39]. Using a 1:60 molar ratio, oleic acid was esterified with methanol at 100, 115, 130 and 160 °C, and the results (Fig. 11) are consistent with the expected behavior. In fact, it is possible that increased temperature was crucial in increasing the conversion in the presence of MF9S4 considerably, from 13.5% at 100 °C to 98.9% at 160 °C.

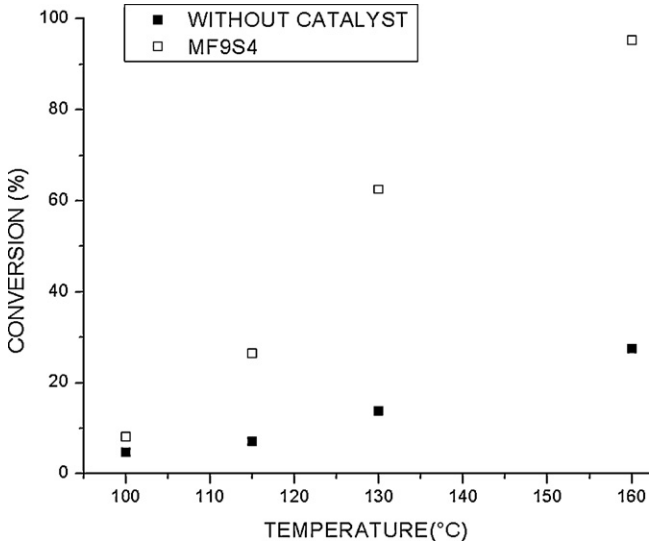

Fig. 11. The effect of temperature on conversion. Acid:alcohol (1:60), time: 120 min.

3.2.4. The effect of the reaction time

The effect of the reaction time was studied using a 1:60 (acid:alcohol) molar ratio at 100, 115, 130 and 160 °C. From the results shown in Fig. 12, it can be observed that the reaction rate increases up to 2 h, after which time the conversion rate increases to a lesser extent. The gradual increase in conversion rate when the reaction time is increased is expected in reactions of esterification [39].Several papers describe first-order kinetics for esterification reactions [19,37,39,40]. In this work, we determined the order of the esterification reaction of oleic acid with methanol using the classical definitions of chemical kinetics and considering oleic acid

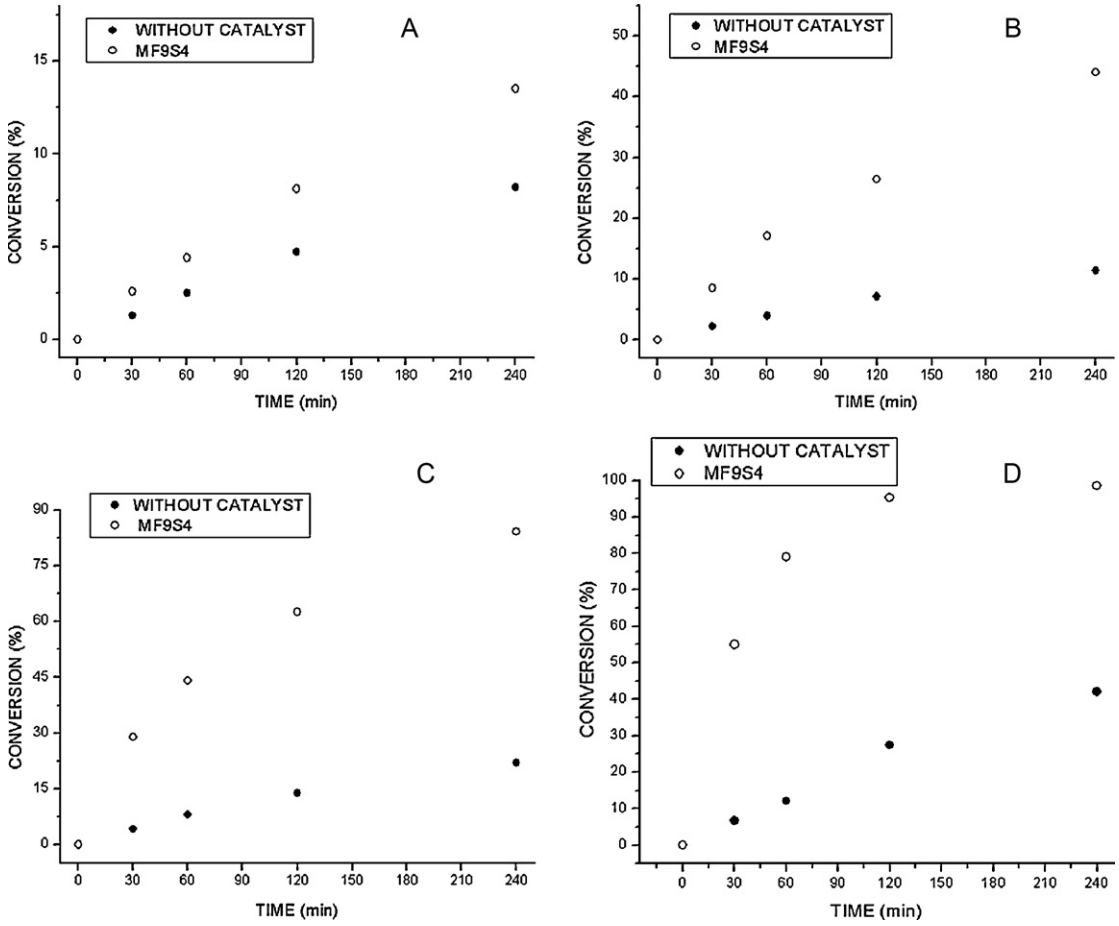

Fig. 12. The effect of time on conversion. Acid:alcohol (1:60), temperature: (A) 100 °C, (B) 115 °C, (C) 130 °C and (D) 160 °C.

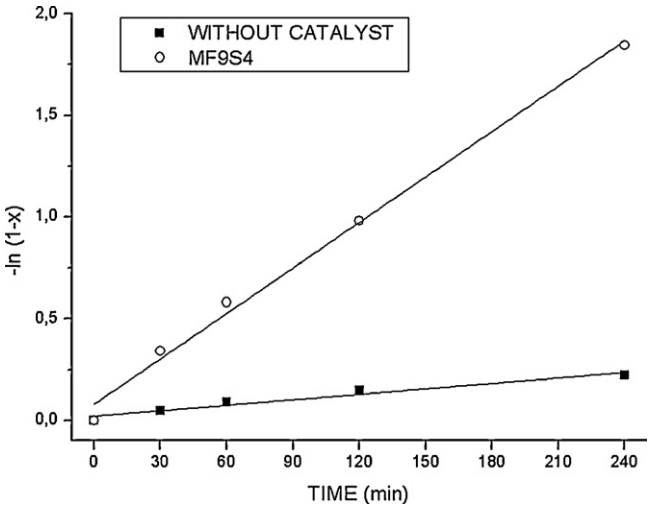

Fig. 13. . The esterification of oleic acid with methanol (1:60, 130 °C). The data fit well to first-order kinetics.

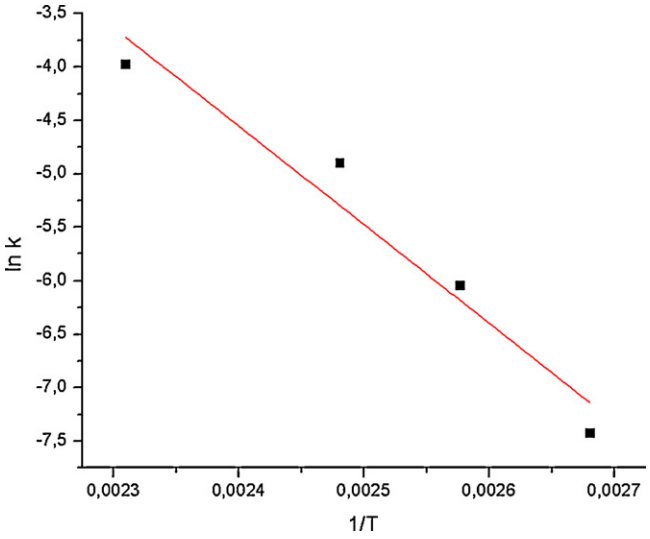

Fig. 14. Arrhenius plot of ln(k) versus 1/T.

as the limiting reagent, whose transformation into esters is followed by the acidity index. To determine the order of the reaction by elementary kinetic theory, we proposed a complete conversion of the acid.Based on Fig. 13, there is a first-order dependence between the reaction rate and the concentration of carboxylic acid for the esterification of oleic acid, as the fitting shows a linear relation between all experimental data when (−ln(1-conversion)) is plotted as a function of the reaction time. The regression coefficients of the straight lines show good fits to first-order kinetics.

Using the esterification conversion data obtained using MF9S4 (Fig. 12), we plotted (−ln(1-conversion)) versus the reaction time (not shown) to calculate the rate constants. The obtained values were 0.000593 at 100 °C, 0.00237 at 115 °C, 0.00745 at 130 °C and 0.01882 at 160 °C. From these values, we plotted the Arrhenius of ln(k) versus 1/T (Fig. 14) and calculated the activation energy and the frequency factor from the Arrhenius equation to be 76.6 kJ/mol and 4.3×10^7 L/mol s, respectively.

Table 4 compares some esterification results found in the literature with those obtained in this work. From the comparison, we can see that the results obtained using MF9S4 as a catalyst for the esterification of oleic acid with methanol are quite satisfactory, because the results are similar to or higher than others presented in the literature [19,39–41], and they also close to the results obtained using homogeneous catalysts at lower temperatures [42,43]. We note that the production cost of the other methods is much higher than the cost of using acid-activated metakaolin prepared from a waste material.

3.2.5. Low quality oil catalyst test

The reaction performance of the MF9S4 was evaluated for the esterification of free fatty acids in a fatty acid/triglyceride mixture. A mixture of 17 wt.% oleic acid in palm oil was used as the model

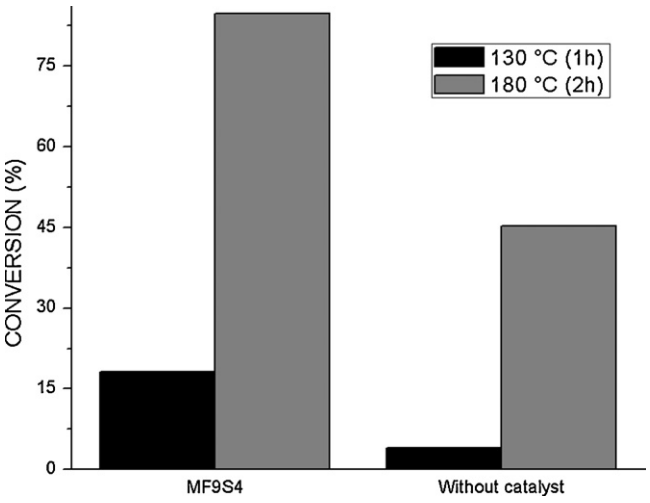

Fig. 15. Relation of conversion of FFA and reaction temperature: reaction time.

high free fatty acid feed. In Fig. 15 it can observed a maximum conversion of 18.2% at a temperature of 130 °C and in a time period of 1 h. The percentage of conversion can be raised by manipulating such variables as time and temperature. For example, at a temperature of 180 °C for a time period of 2 h, the removal of FFA observed is 84.8%. This value is greater than those presented by other types of heterogeneous catalysts reported in the literature. For instance, when organosulfonic acid-functionalized mesoporous silica [22] was used in the esterification of fatty acids, the reaction reached approximately 80% of conversion of fatty acids to methyl esters. The same kind of reaction reached 60% of conversion when Al-MCM-41

Table 4
The esterification reaction using different catalysts.

Acid	Alcohol	Alcohol/acid	Temp. (°C)	Catalyst	Conversion (%)	Ref.
Acetic	n-Butanol	1/2	125	Al-MCM-41 (Si/Al = 25)	87.3	[41]
Acetic	n-Propanol	1/2	150	Al-MCM-41 (Si/Al = 30)	83.7	[39]
Acetic	Amyl	1/2	250	Al-MCM-41 (Si/Al = 100)	91.0	[40]
Palmitic	Methanol	60/1	130	Al-MCM-41 (Si/Al = 8)	79.0	[19]
Oleic	Methanol	3	80	H_2SO_4	91	[42]
Palmitic	Methanol	5	130	*p*-Toluene sulfonic acid	94.5	[43]
Oleic	Methanol	60/1	130	MF9S4	84.2	[a]
Oleic	Methanol	60/1	160	MF9S4	98.9	[a]

[a] Present work.

was applied. [19]. Compared to organosulfonic acid-functionalized mesoporous silicas and MCM-41, the activated metakaolin seems to be a more attract catalyst for pretreatment process of low quality oils, due to its simple and low cost processes of preparation.

4. Conclusions

We studied the catalytic applications of Amazon *flint* kaolin for the first time. The different treatments to which the *flint* kaolin was submitted resulted in microporous materials with different textural and physicochemical properties. Thermal activation at 950 °C made the *flint* kaolin more reactive and susceptible to acid leaching.

Some activated metakaolins presented a considerable increase of the superficial area, in addition to the high microporous volume that is related to the spaces observed by SEM and the amount of amorphous silica. The presence of both Brönsted and Lewis acidic sites were confirmed in the acid-activated metakaolins by the acidity evaluation, with MF9S4 presenting the higher values.

MF9S4 was the best catalyst for the esterification of oleic acid with methanol, reaching 98.9% of conversion rate at 160 °C, an acid:methanol molar ratio of 1:60 and 4 h reaction time. The performance of MF9S4 is related directly to its having the largest surface area and to the density of its acid sites. MF9S4 also seems to be an alternative for removal of free fatty acids from low quality oils.

The results obtained at this work indicate that a waste material, Amazon *flint* kaolin, can be considered a promising raw material for the production of a new eco-friendly catalyst for the esterification of FFAs, providing an alternative route for production of sustainable fuels.

Acknowledgments

The authors thank CNPq, SEDUC/CAPES, PRONEX/FAPESPA and LAPAC/UFPA for financial support.

References

[1] A. Vaccari, Catal. Today 41 (1998) 53–71.
[2] A. Vaccari, Appl. Clay Sci. 14 (1999) 161–198.
[3] M.J.C Rezende, Ph.D. Thesis, UFRJ, Rio de Janeiro, Brasil. Unpublished results.
[4] M. Lenarda, L. Storaro, A. Talon, E. Moretti, P. Riello, J. Colloid Interface Sci. 311 (2007) 537–543.
[5] D.M. Araújo Melo, J.A.C. Ruiz, M.A.F. Melo, E.V. Sobrinho, M. Schmall, Microporous Mesoporous Mater. 38 (2000) 345–349.
[6] J.L. Venaruzzo, C. Volzone, M.L. Rueda, J. Ortiga, Microporous Mesoporous Mater. 56 (2002) 73–80.
[7] U. Flessner, D.J. Jones, J. Rozière, J. Zajac, L. Storaro, M. Pavan, A. Jiménez-López, E. Rodríguez-Castellón, M. Trombetta, G. Busca, J. Mol. Catal. A: Chem. 168 (2001) 247–256.
[8] C. Belver, M.A.B. Muñoz, M.A. Vicente, Chem. Mater. 14 (2002) 2033–2043.
[9] M.P. Hart, D.R. Brown, J. Mol. Catal. A: Chem. 212 (2004) 315–321.
[10] M. Perissinotto, M. Lenarda, L. Storaro, R. Ganzerla, J. Mol. Catal. A: Chem. 121 (1997) 103–109.
[11] K.R. Sabu, R. Sukumar, R. Rekha, M. Lalithambika, Catal. Today 49 (1999) 321–326.
[12] G. Centi, S. Perathoner, Microporous Mesoporous Mater. 107 (2008) 3–15.
[13] B.S. Carneiro, R.S. Angélica, T. Scheller, E.A.S. de Castro, R.F. Neves, Cerâmica 49 (2003) 237–244.
[14] D.J.L. Souza, MSc. Thesis UFPA, Belém, Brasil. Unpublished results.
[15] B. Kotschoubey, W. Truckenbrodt, B. Hieronymus, Rev. Bras. Geociênc. 26 (2) (1996) 71–80.
[16] K. Jacobson, R. Gopinath, L.C. Meher, A.K. Dalai, Appl. Catal. B 85 (2008) 86–91.
[17] N. Boz, N. Degirmenbasi, D.M. Kalyon, Appl. Catal. B 89 (2009) 590–596.
[18] S. Zheng, M. Kates, M.A. Dubé, D.D. McLean, Biomass Bioenergy 30 (2006) 267–272.
[19] A.C. Carmo Jr., L.K.C. de Souza, C.E.F. da Costa, E. Longo, J.R. Zamian, G.N. da Rocha Filho, Fuel 88 (2009) 461–468.
[20] K. Srilatha, N. Lingaiah, B.L.A. Prabhavathi Devi, R.B.N. Prasad, S. Venkateswar, P.S. Sai Prasad, Appl. Catal. A 365 (2009) 28–33.
[21] J.M. Marchetti, A.F. Errazu, Biomass Bioenergy 32 (2008) 892–895.
[22] I.K. Mbaraka, D.R. Radu, V.S.-Y. Lin, B.H. Shanks, J. Catal. 219 (2003) 329–336.
[23] R. Liu, X. Wang, X. Zhao, P. Feng, Carbon 46 (2008) 1664–1669.
[24] X. Mo, E. Lotero, C. Lu, Y. Liu, J.G. Goodwin, Catal. Lett. 123 (2008) 1–6.
[25] D.E. López, J.G. Goodwin Jr., D.A. Bruce, S. Furuta, Appl. Catal. A 339 (2008) 76–83.
[26] K.N. Rao, A. Sridhar, A.F. Lee, S.J. Tavener, N.A. Young, K. Wilson, Green Chem. 8 (2006) 790.
[27] I.K. Mbaraka, B.H. Shanks, J. Catal. 244 (2006) 78–85.
[28] L. Xu, W. Li, J. Hu, X. Yang, Y. Guo, Appl. Catal. B 90 (3–4) (2009) 587–594.
[29] G.F. Ghesti, J.L. de Macedo, V.C.I. Parente, J.A. Dias, S.C.L. Dias, Microporous Mesoporous Mater. 100 (2007) 27–34.
[30] V. Rives, Catal. Today 56 (2000) 357–359.
[31] D.J. Parrillo, A.T. Adamo, G.T. Kokotailo, R.J. Gorte, Appl. Catal. 67 (1990) 107–118.
[32] S.B. Sharma, B.L. Meyers, D.T. Chen, J. Miller, J.A. Dumesic, Appl. Catal. A 102 (1993) 253–265.
[33] V.L. Zholobenko, D. Plant, A.J. Evans, S.M. Holmes, Microporous Mesoporous Mater. 44–45 (2001) 793–799.
[34] E.P. Parry, J. Catal. 2 (1963) 371–379.
[35] J. Konta, Appl. Clay Sci. 10 (1995) 275–335.
[36] S.R. Chitnis, M.M. Sharma, Reaja, Funct. Polym. 32 (1997) 93–115.
[37] S.R. Kirumakki, N. Nagaraju, K.V.R. Chary, Appl. Catal. A 299 (2006) 185–192.
[38] A. Zaidi, J.L. Gainer, G. Carta, A. Mrani, T. Kadiri, Y. Belarbi, A. Mir, J. Biotechnol. 93 (2002) 209–216.
[39] N. Gokulakrishnan, A. Pandurangan, P.K. Sinha, J. Mol. Catal. A: Chem. 263 (2007) 55–61.
[40] A. Palani, A. Pandurangan, J. Mol. Catal. A: Chem. 226 (2005) 129–134.
[41] B.R. Jermy, A. Pandurangan, Appl. Catal. A 288 (2005) 25–33.
[42] J.-Y. Park, Z.-M. Wang, D.-K. Kim, J.-S. Lee, Renew. Energy 35 (2010) 614–618.
[43] R. Aafaqi, A.R. Mohamed, S. Bhatia, J. Chem. Technol. Biotechnol. 79 (2004) 1127–1134.